ACS APPLIED MATERIALS & INTERFACES

Research Article

www.acsami.org

Titanium Sulfides as Intercalation-Type Cathode Materials for Rechargeable Aluminum Batteries

Linxiao Geng,[†] Jan P. Scheifers,[‡] Chengyin Fu,[†] Jian Zhang,[§] Boniface P. T. Fokwa,[‡,§] and Juchen Guo*[,†,§]

[†]Department of Chemical and Environmental Engineering, University of California, Riverside, California 92521, United States

[‡]Department of Chemistry, University of California, Riverside, California 92521, United States

[§]Materials Science and Engineering Program, University of California, Riverside, California 92521, United States

Supporting Information

ABSTRACT: We report the electrochemical intercalation−extraction of aluminum (Al) in the layered TiS_2 and spinel-based cubic $Cu_{0.31}Ti_2S_4$ as the potential cathode materials for rechargeable Al-ion batteries. The electrochemical characterizations demonstrate the feasibility of reversible Al intercalation in both titanium sulfides with layered TiS_2 showing better properties. The crystallographic study sheds light on the possible Al intercalation sites in the titanium sulfides, while the results from galvanostatic intermittent titration indicate that the low Al^{3+} diffusion coefficients in the sulfide crystal structures are the primary obstacle to facile Al intercalation−extraction.

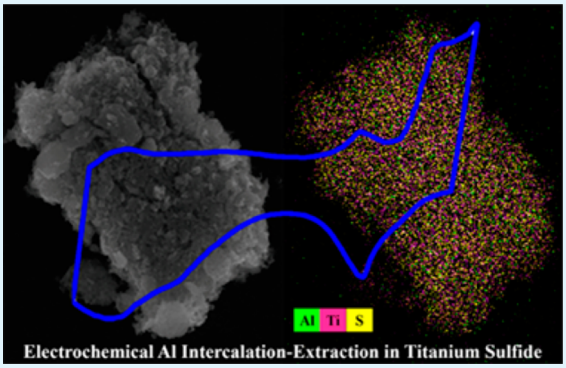

KEYWORDS: *aluminum-ion battery, aluminum intercalation, multivalent ion battery, titanium sulfides, ionic liquid electrolyte*

INTRODUCTION

The rechargeable aluminum-ion (Al-ion) battery is an intriguing electrochemical energy storage technology based on the most abundant metal in the earth's crust. It can be a potentially interruptive technology for large scale energy storage applications.[1] However, reversible electrochemical processes involving Al are inherently difficult. One challenge is the lack of feasible electrolytes for Al deposition−dissolution at the anode. The most commonly adopted Al electrolytes to date are Lewis acidic mixtures of aluminum halides (AlX_3, X = Cl and Br) and halide-containing ionic liquids (ILs), such as 1-butylpyridinium chloride and 1-ethyl-3-methylimidazolium chloride, with molar ratio > 1.[2,3] Halide-free IL electrolyte[4] and aqueous $AlCl_3$ electrolytes[5,6] have also been reported. Another challenge comes from the lack of understanding of cathode materials. With increasing interest, a few potential cathode materials have been proposed based on various reaction mechnisms.[7−17] Transition metal oxides, particularly vanadium(V) oxide (V_2O_5), were studied as intercalation-type cathode materials.[10−14] Lin and co-workers proposed graphitic carbon as a possible cathode material based on an anion intercalation mechnism.[15] Archer's and Wang's groups also presented the possibility of sulfur as a cathode material based on a redox conversion reaction.[8,9]

We previously reported the Chevrel phase molybdenum sulfide (Mo_6S_8) as an intercalation-type metal sulfide cathode material.[16] An independent investigation by Lee and co-workers further confirmed the reversible electrochemical Al intercalation in Mo_6S_8.[17] Our selection of transition metal sulfides in place of oxides as Al-ion cathode materials is crucial: Due to the strong Coulombic effect, the energy barrier for multivalent ion transport in the oxide crystal structure is high.[18] Therefore, a more polarizable (softer) anionic framework is needed for facile Al^{3+} ion intercalation−extraction, making transition metal sulfides promising candidates as Al-ion cathode materials. Although Mo_6S_8 showed unambiguous electrochemical Al intercalation−extraction properties, its specific capacity was not ideal due to its high molecular mass. We herein report the Al intercalation−extraction properties of two titanium sulfides, layered TiS_2 and spinel-based, cubic $Cu_{0.31}Ti_2S_4$, as potential intercalation-type cathode materials for Al-ion batteries.

EXPERIMENTAL SECTION

Synthesis of Layered TiS_2. Layered TiS_2 was synthesized via solid state reaction by heating stoichiometric mixture of the elements (Ti and S).[19] Stoichiometric amounts of Ti powder (Alfa Aesar, 325 mesh, 99.5%) and S powder (Sigma-Aldrich 99.5−100.5%) were thoroughly mixed and then sealed in an evacuated quartz tube, which was subsequently heated in a muffle furnace. The temperature was first ramped up to 450 °C at a rate of 0.3 °C min^{-1} and then held at 450 °C for 24 h, after which the temperature was ramped up to 640 °C in 24 h and held at 640 °C for 3 days. The synthesized TiS_2 was collected in

Received: March 23, 2017
Accepted: June 1, 2017
Published: June 1, 2017

DOI: 10.1021/acsami.7b04161
ACS Appl. Mater. Interfaces 2017, 9, 21251−21257

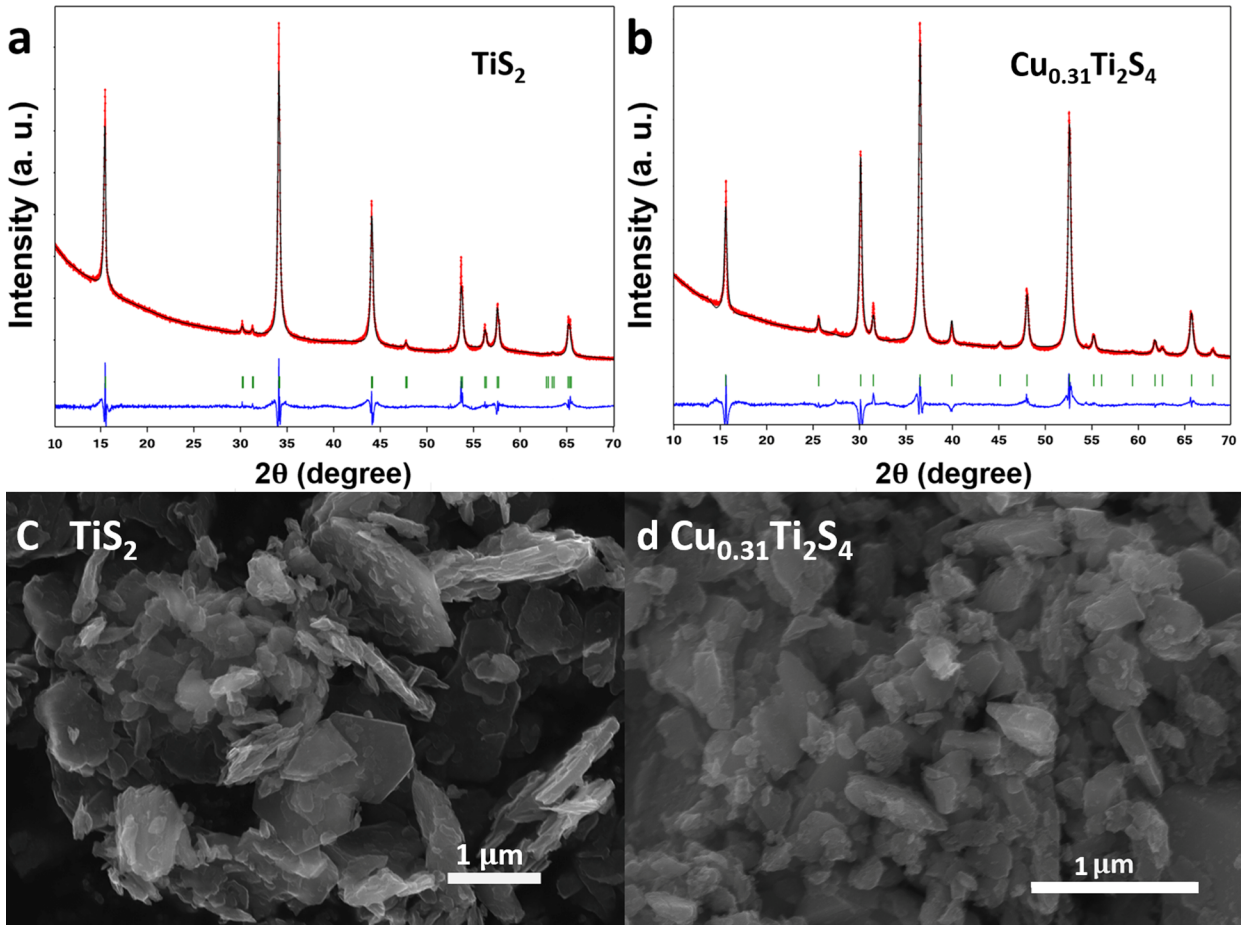

Figure 1. XRD patterns and Rietveld refinements of layered TiS_2 (a) and cubic $Cu_{0.31}Ti_2S_4$ (b); SEM images of layered TiS_2 (c) and cubic $Cu_{0.31}Ti_2S_4$ (d).

an argon-filled glovebox to prevent oxidization and hydrolysis. Mechanical ball milling was employed to reduce the particle size of TiS_2 with a Fritsch Pulverisette 23 mini-Mill. The entire ball milling process was performed in the argon-filled glovebox. In a typical ball milling process, two 10 mm diameter and 18 5 mm diameter tempered steel grinding balls along with 0.346 g of TiS_2 (weight ratio 50:1) were put into a tempered steel grinding bowl with 3 mL of anhydrous toluene. To prevent overheating, the milling was performed in 10 sessions of 5 min, each separated by 10 min of idling. After the ball milling, the TiS_2 particles were washed with anhydrous acetonitrile 3 times and then collected with a centrifuge. The scanning electron microscopy (SEM) image and the powder X-ray diffraction (XRD) pattern of the pristine TiS_2 are shown in the Supporting Information (Figure S1) with the energy dispersive X-ray spectroscopy (EDS) elemental mapping of the TiS_2 after ball milling (Figure S2 and Table S1).

Synthesis of Cubic $Cu_{0.31}Ti_2S_4$. Thiospinel $CuTi_2S_4$ was first synthesized using a solid state method similar to that described above.[20] Stoichiometric amounts of Cu (Sigma-Aldrich, 14−25 μm, 99%), Ti, and S powders were thoroughly mixed and sealed in an evacuated quartz tube. The quartz tube was heated in a muffle furnace at 700 °C (ramp rate, 0.3 °C min^{-1}) for 3 days. The synthesized $CuTi_2S_4$ was collected in the argon-filled glovebox to prevent oxidization and hydrolysis. The particle size of $CuTi_2S_4$ was reduced via mechanical ball milling as described above. Cu was leached from the $CuTi_2S_4$ product by reaction with bromine. In a typical leaching process, 300 mg of $CuTi_2S_4$ was suspended in 100 mL of anhydrous acetonitrile. Then, 94 μL of pure bromine was added to the suspension. The mixture was stirred for 24 h. After the reaction, the product was washed twice with both acetonitrile and carbon disulfide and collected with a centrifuge. The chemical formula of the product was determined to be $Cu_{0.31}Ti_2S_4$ via XRD analysis and Rietveld refinement and was confirmed by EDS elemental mapping. The SEM images and the XRD patterns of $CuTi_2S_4$ before and after ball milling are shown in the Supporting Information (Figure S3) with the EDS element analysis of the synthesized $Cu_{0.31}Ti_2S_4$ (Figure S4 and Table S2).

Electrochemical Analysis. CR2016 coin cells were assembled in an argon-filled glovebox using Al foil (0.2 mm thickness, Alfa Aesar, 99.9999%) as the anode. The cathode was fabricated by coating TiS_2 or $Cu_{0.31}Ti_2S_4$ slurry onto a carbon paper current collector (Spectracarb 2050A-0550, Fuel Cell Store). The carbon paper current collector was demonstrated to be electrochemically inert in the applied potential window as shown in the Supporting Information (Figure S5). The slurry was made by mixing 80 wt % TiS_2 or $Cu_{0.31}Ti_2S_4$, 10 wt % carbon black, and 10 wt % polystyrene in *N*-methyl-2-pyrrolidone via a mechanical mixer for 5 min. A single Whitman glass fiber filter was used as the separator. The electrolyte was prepared by slowly adding anhydrous $AlCl_3$ (Sigma-Aldrich, 99.99%) into 1-butyl-3-methylimidazolium chloride (Sigma-Aldrich, 98%) with a molar ratio of 1.5:1 while stirring in the argon-filled glovebox. It is worth noting that polystyrene was selected as the binder due to its inertness in the Lewis acidic ionic liquid electrolyte compared to conventional binders such as poly(vinylidene fluoride) (Figure S6 in the Supporting Information). To prevent corrosion from the acidic electrolyte, titanium foil (Strem, 0.025 mm thickness, 99.6%) and pyrolytic graphite sheet (MTI, 0.017 mm thickness, 99.90%) were punched into discs of an appropriate size to be used as linings in the stainless-steel coin cell case. The schematic of the coin cell construction is shown in Supporting Information (Figure S7). Cyclic voltammetry (CV) with a scan rate of 0.1 mV s^{-1} was performed with a Gamry potentiostat Interface 1000. Galvanostatic discharging and constant-current−

DOI: 10.1021/acsami.7b04161
ACS Appl. Mater. Interfaces 2017, 9, 21251−21257

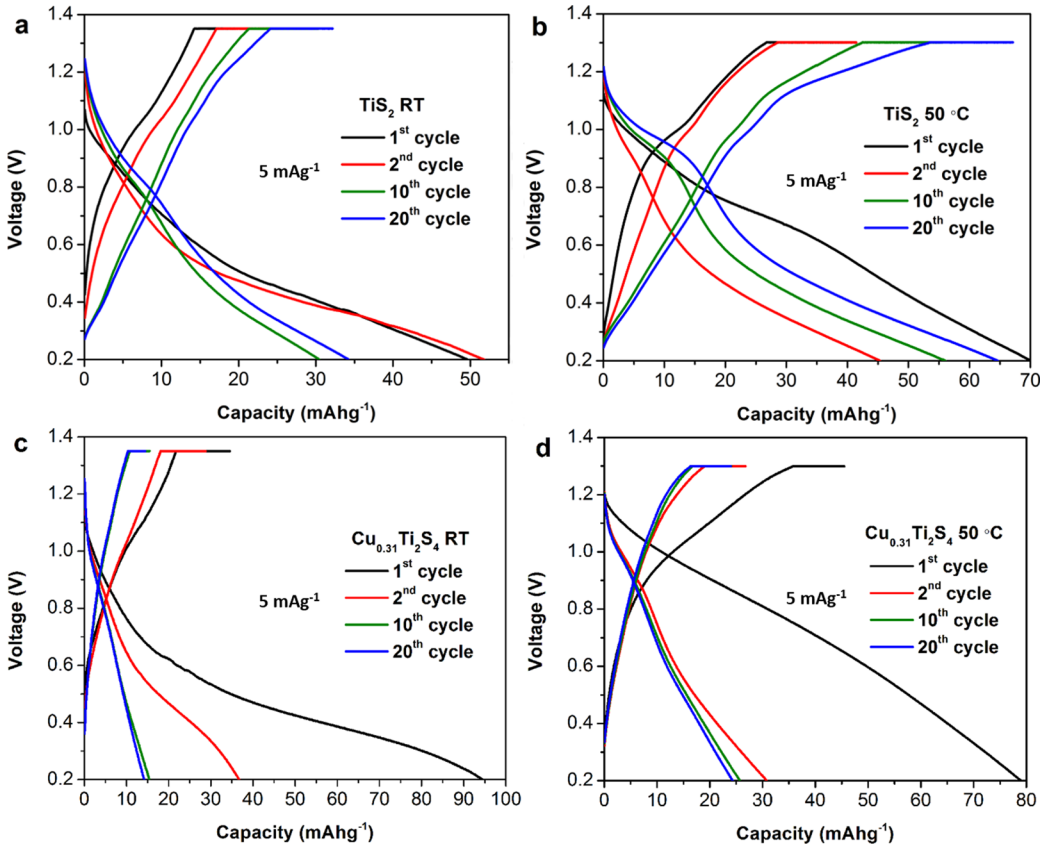

Figure 2. First, second, 10th, and 20th galvanostatic discharge and CCCV charge curves of layered TiS_2 (a and b) and cubic $Cu_{0.31}Ti_2S_4$ (c and d) at RT and 50 °C.

constant-voltage (CCCV) charging and galvanostatic intermittent titration technique (GITT) were performed on an Arbin battery test station. In GITT, the batteries were discharged and charged at 10 mA g^{-1} for 15 min and rested for 2 h. The current pulse was repeated until the potential reached the cutoff limit. The diffusion coefficient of Al^{3+} was calculated according to the following equation:

$$D = \frac{4}{\tau}\left(\frac{IV_M}{Z_A FS}\right)^2 \left[\frac{\left(\frac{dE}{dx}\right)}{\left(\frac{dE}{d\sqrt{t}}\right)}\right]^2$$

where D is the Al^{3+} ion diffusion coefficient, I is the current used in titration, V_M is the molar volume of the titanium sulfides, Z_A is the number of charge of the ionic species (Z_A = 3 for Al^{3+}), F is the Faraday constant, S is the surface area of the active materials (53.1 m^2 g^{-1} for layered TiS_2 and 27.2 m^2 g^{-1} for cubic $Cu_{0.31}Ti_2S_4$, determined by N_2 adsorption−desorption experiments), x is the content of Al in the electrode materials (Al_xTiS_2 and $Al_xCu_{0.31}Ti_2S_4$), and τ is the current pulse time. The value of $dE/d\sqrt{t}$ is determined from the plot of the voltage response vs the square root of the time during each current pulse, and dE/dx is obtained by plotting the equilibrium potential vs the electrode material composition after each current pulse.[21]

Materials Characterizations. The XRD was conducted using a PANalytical EMPYREAN instrument (45 kV/40 mA) with a Cu Kα source. SEM was performed with a FEI XL30-FEG instrument. The N_2 adsorption−desorption isotherms for surface area measurements were obtained with Micromeritics ASAP 2020 apparatus.

RESULTS AND DISCUSSION

As shown in Figure 1a, the XRD pattern of the synthesized TiS_2 matched the reference very well. As the XRD and the Rietveld refinement data show in Figure 1b, the final product of chemically leached $CuTi_2S_4$ had a formula of $Cu_{0.31}Ti_2S_4$. The particle size of TiS_2 (diameter of the plate-like particle) and $Cu_{0.31}Ti_2S_4$ obtained from SEM images (Figure 1c,d) was mostly smaller than 1 μm.

The electrochemical Al intercalation−extraction in these two titanium sulfides were characterized with discharge−charge experiments at both room temperature (RT) and 50 °C considering the slow intercalation kinetics observed in the Chevrel phase Mo_6S_8 at RT.[16,22] Galvanostatic discharge (Al intercalation) was carried out by applying 5 mA g^{-1} current density, and the same current density was applied first for the galvanostatic charge (Al extraction), followed by holding a constant potential of 1.35 V (RT) and 1.3 V (50 °C) vs Al, respectively, for 3 h. This constant-current−constant-voltage (CCCV) charge protocol was used to prevent the corrosion (electrochemical oxidation) of the linings and the stainless-steel cell case from the acidic IL electrolyte. CCCV charging is also a common practice to overcome the kinetic voltage polarization to achieve more complete ion extraction. Figure 2 shows the galvanostatic discharge and CCCV charge curves of TiS_2 and $Cu_{0.31}Ti_2S_4$ at the first, second, 10th, and 20th cycles at RT and 50 °C. It is clear that the Al interaction−extraction behaviors of either titanium sulfide are inherently the same at the different temperatures used. However, higher capacity and more distinct discharge−charge characteristics are demonstrated at 50 °C due to the improved reaction kinetics at higher temperature. As shown in Figure 2b, the first discharge curve of TiS_2 at 50 °C displays a plateau at 0.75 V followed by a slope from 0.6 to 0.2 V with a total capacity of 70 mA h g^{-1}. However, the first charge capacity is only 40 mA h g^{-1}, indicating a high

DOI: 10.1021/acsami.7b04161
ACS Appl. Mater. Interfaces 2017, 9, 21251−21257

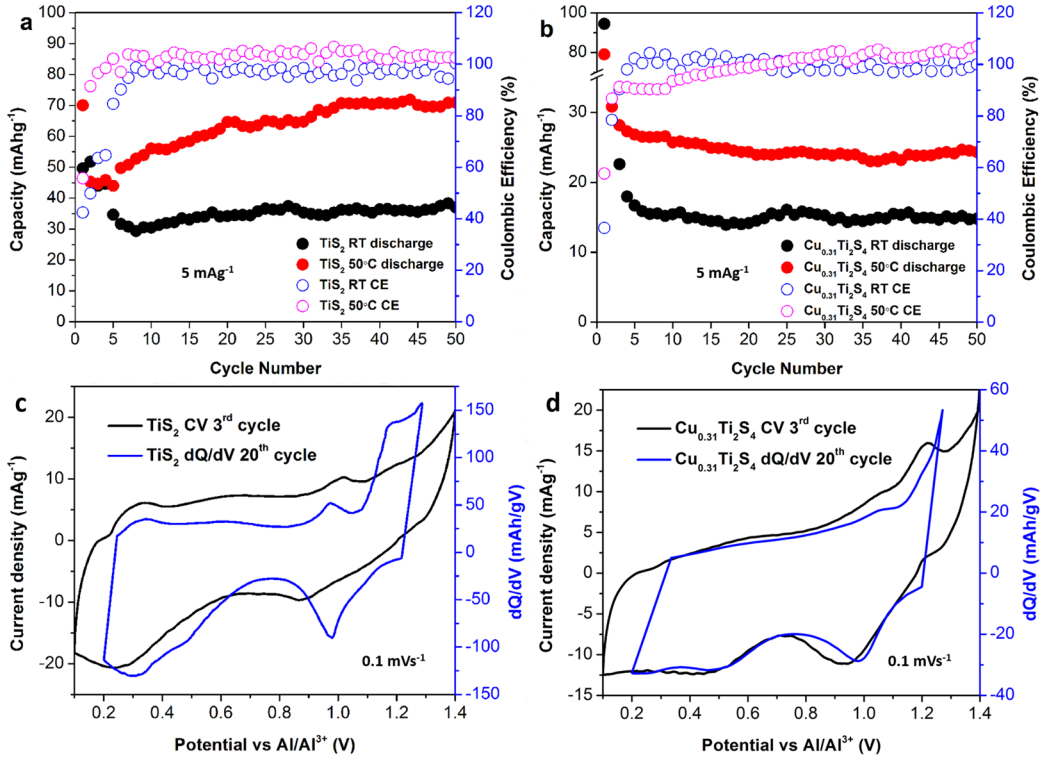

Figure 3. Cycle stabilities of layered TiS_2 (a) and cubic $Cu_{0.31}Ti_2S_4$ (b) at room temperature and 50 °C with 5 mA g^{-1} current density. Cyclic voltammetry and differential capacity curves of TiS_2 (c) and $Cu_{0.31}Ti_2S_4$ (d) at 50 °C.

irreversibility in the first cycle. During the following cycles, the discharge−charge potential profile gradually evolves with increasing capacity. Two discharge stages can still be observed in the stabilized discharge curve with a plateau around 0.95 V and a slope from 0.6 to 0.2 V. We hypothesize that the Al intercalation−extraction process in the initial cycles slightly altered the crystal structure of TiS_2, thus facilitating the Al intercalation−extraction in the subsequent cycles. Figure 2d shows the galvanostatic discharge and CCCV charge curves of cubic $Cu_{0.31}Ti_2S_4$ at 50 °C. One can observe a slope-like discharge curve from the first discharge with a capacity around 80 mA h g^{-1}. The first charge also displays a slope-like potential curve with a capacity of 45 mA h g^{-1}. Unlike layered TiS_2, the discharge−charge capacity of $Cu_{0.31}Ti_2S_4$ does not recover during the following cycles. Instead, the discharge−charge potential profile of $Cu_{0.31}Ti_2S_4$ stabilizes after 10 cycles with a modest reversible capacity of 25 mA h g^{-1}.

The cycle stability of layered TiS_2 and cubic $Cu_{0.31}Ti_2S_4$ are shown in Figure 3a,b. The reversible capacity of layered TiS_2 at 50 °C is significantly higher than that at RT: the capacity gradually increases after the first few cycles and stabilizes at approximately 70 mA h g^{-1}. On the other hand, the reversible capacity of cubic $Cu_{0.31}Ti_2S_4$ at 50 °C is only about 25 mA h g^{-1}. From the capacity comparison of these two titanium sulfides, it can be speculated that more Al can be reversibly intercalated in layered TiS_2 than in cubic $Cu_{0.31}Ti_2S_4$. This hypothesis can be attributed to the fact that the channels in the spinel structure are more rigid and less open than those of the layered structure, thus making the material less adaptive to accommodating the intercalated Al^{3+} ions. The high irreversible capacity in the first cycle of both titanium sulfides may be due to the irreversible Al intercalation (Al^{3+} ions trapped in the crystal structures). It is also worth noting that the Coulombic efficiency at 50 °C for both sulfides is higher than 100%, which may be caused by the gradual electrochemical or chemical corrosion of the Al anode during discharge, while the protective linings and the coin cell case remain corrosion-free (Figures S8−S11 in the Supporting Information). The SEM and EDS analysis of the electrodes after 50 cycles demonstrates the consistent chemical composition with the initial materials (Figures S12 and S13 and Tables S3 and S4 in the Supporting Information). Electrolyte decomposition, i.e., possible solid electrolyte interphase formation, was not observed on either titanium sulfide using X-ray photoelectron spectroscopy (XPS) analysis (Figure S14 in the Supporting Information). It is also worth mentioning that exposure to the ambient environment can quickly form an oxide layer on the surface of both titanium sulfides, which is detrimental to Al intercalation. The surface XPS analysis of the air exposed titanium sulfides and the resulting capacity tests are described in the Supporting Information (Figure S15).

To identify the Al intercalation−extraction potential, the differential capacity curves (dQ/dV) of TiS_2 and $Cu_{0.31}Ti_2S_4$ at 50 °C are plotted in Figure 3c,d alongside the corresponding CV curves (complete CV cycles are shown Figure S16 in the Supporting Information). The dQ/dV and CV curves agree strongly with each other. Figure 3c clearly displays two pronounced cathodic (intercalation) peaks for layered TiS_2 at approximately 0.98 and 0.3 V and two anodic (extraction) peaks at 0.97 and 1.15 V. On the other hand, $Cu_{0.31}Ti_2S_4$ (Figure 3d) displays two broad and less pronounced cathodic peaks at 1.0 and 0.5 V; two broad anodic peaks with very low peak currents can barely be distinguished at 0.6 and 1.2 V, indicating the inferior intercalation−extraction kinetics of cubic $Cu_{0.31}Ti_2S_4$.

To confirm the intercalation of Al into the crystal structure of layered TiS_2 and cubic $Cu_{0.31}Ti_2S_4$, Rietveld refinements were performed on the powder XRD data of the Al-intercalated

DOI: 10.1021/acsami.7b04161
ACS Appl. Mater. Interfaces 2017, 9, 21251−21257

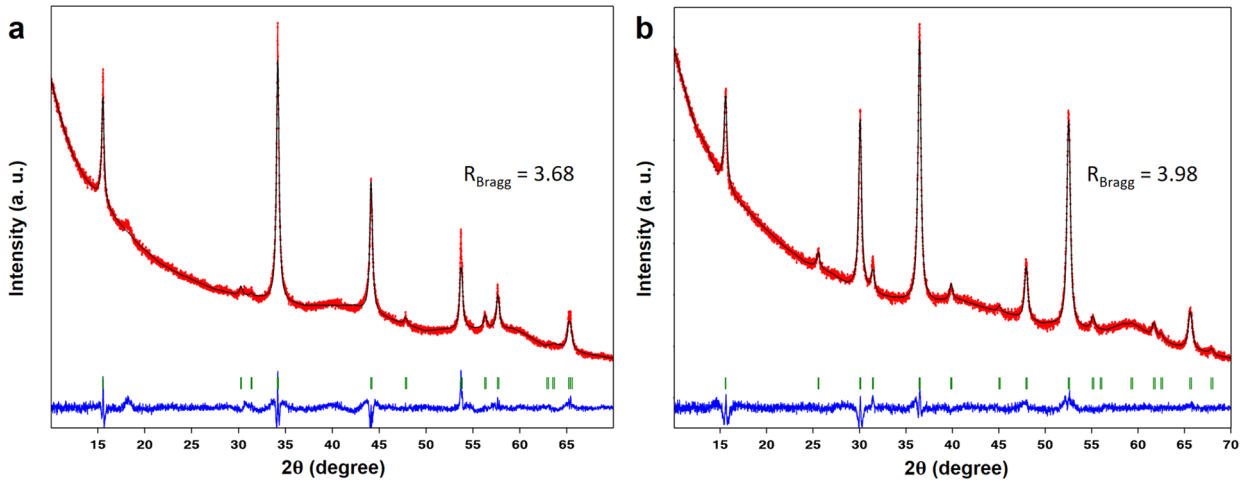

Figure 4. XRD patterns and Rietveld refinements of Al-intercalated layered TiS_2 (a) and Al-intercalated cubic $Cu_{0.31}Ti_2S_4$ (b).

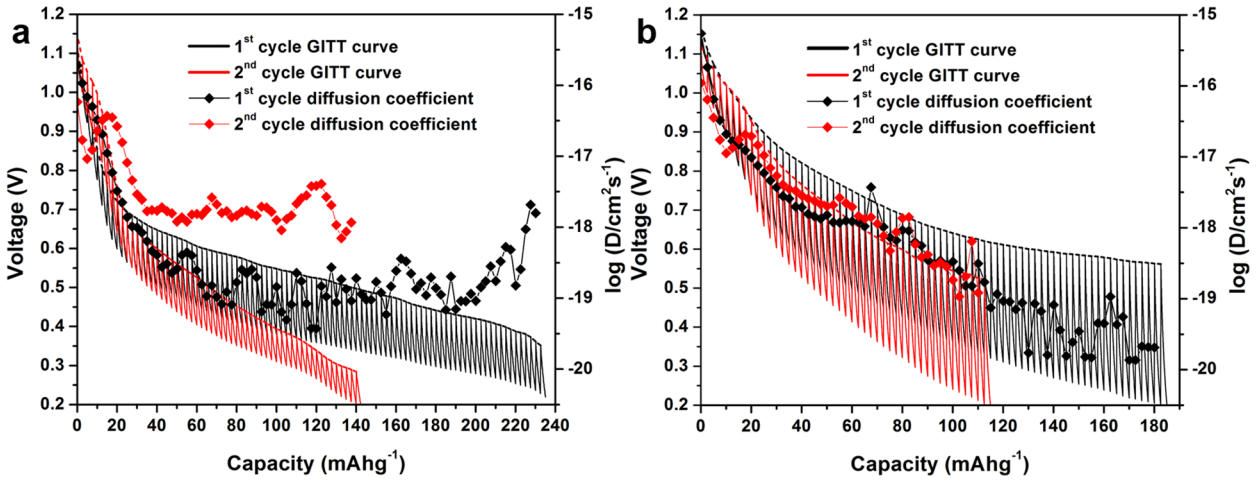

Figure 5. Galvanostatic intermittent titration technique (GITT) curve of layered TiS_2 (a) and cubic $Cu_{0.31}Ti_2S_4$ (b) at 50 °C.

titanium sulfides, which were obtained from chronopotentiometry with a small current density of 2 mA g^{-1} at 50 °C (Figure S17 in the Supporting Information). Figure 4a shows the refinement result of Al-intercalated TiS_2. TiS_2 and Al-intercalated TiS_2 crystallized in space group $P\bar{3}m1$. The unit cell parameters of Al-intercalated TiS_2, $a = b = 3.4106(8)$ Å and $c = 5.703(2)$ Å, are, surprisingly, smaller than those for pristine TiS_2. Consequently, the volume of the unit cell decreases upon intercalation, and there is an additional reflection at 18.2°. We hypothesize that this additional reflection could indicate Al ordering and consequently an ordered superstructure. The decreased lattice parameter could be caused by the very small, highly charged Al^{3+} ions in the van der Waals gap reducing the repulsion between the S-layers in TiS_2. The position of Al^{3+} in the unit cell used for the refinement is (0, 0, 0.5), which is the position 1b with octahedral coordination between the S-layers. We also attempted to refine Al^{3+} on the tetrahedral site 2d. This increased the Al^{3+} concentration, but the quality of the refinement did not improve significantly. Due to short S−Al distances and the limited available space, whether Al occupies the tetrahedral site remains questionable. Thus, the final result of the refinement is that Al occupies 11% of the octahedral intercalation positions 1b which corresponds to a composition of $Al_{0.11(1)}TiS_2$. Upon calculating the electrochemical capacity from the composition information, we derive a capacity of about 79 mA h g^{-1}, which is in good agreement with the electrochemical experimental results. The Rietveld refinement of Al-intercalated cubic $Cu_{0.31}Ti_2S_4$ is shown in Figure 4b. The spinel-type structure has the space group structure $Fd\bar{3}m$. The unit cell parameters of Al-intercalated cubic $Cu_{0.31}Ti_2S_4$ are $a = b = c = 9.855(1)$ Å, which is approximately 1% smaller than $CuTi_2S_4$ but larger than $Cu_{0.31}Ti_2S_4$ ($a = b = c = 9.834(2)$ Å). In order to perform the refinement on Al-intercalated $Cu_{0.31}Ti_2S_4$, the following assumptions are made: (1) Al^{3+} occupies the same position as Cu^+; (2) the amount of Cu^+ does not change during the intercalation process. The refinement yields that Al occupies 9% of the intercalation positions, resulting in a composition of $Al_{0.09(1)}Cu_{0.31}Ti_2S_4$. This yields a capacity of about 32 mA h g^{-1} based on composition, which is also in good agreement with the electrochemical experimental results.

Based on the findings described above, we speculate that the difficulty of Al interaction in both titanium sulfides is imposed by the kinetic limitation: The energy barrier for Al intercalation in both titanium sulfides comes from the strong Coulombic attraction between the Al^{3+} cations and the sulfide anion framework. Thus, the near-equilibrium Al intercalation properties of these two titanium sulfides were studied with GITT at 50 °C. The GITT curve of the first Al intercalation in layered TiS_2 (Figure 5a) shows a much higher capacity than the one obtained by galvanostatic discharge (Figure 2b) due to the

DOI: 10.1021/acsami.7b04161
ACS Appl. Mater. Interfaces 2017, 9, 21251−21257

relaxation of potential to equilibrium after pulse titration. The GITT capacity of 235 mA h g^{-1} in the first intercalation indicates one electron transfer per TiS_2 ($Al_{1/3}TiS_2$). However, the capacity GITT demonstrates in the second Al intercalation is significantly reduced to 140 mA h g^{-1}, which suggests large irreversibility of Al^{3+} trapped in the TiS_2 crystal structure. The equilibrium Al intercalation potential curve displays solid solution type of behavior. Therefore, the Al^{3+} diffusion coefficient in layered TiS_2 at 50 °C can be calculated from the GITT data as a function of intercalation capacity (i.e., Al content in the intercalated TiS_2). The Al^{3+} diffusion coefficient is in the range of 10^{-18} to 10^{-19} cm^2 s^{-1} in the first intercalation cycle. Interestingly, the Al^{3+} diffusion coefficient increases by 1 order of magnitude in the second intercalation cycle, which may be due to the structural change of TiS_2 induced by the initial Al intercalation. Figure 5b shows the GITT data of Al intercalation in cubic $Cu_{0.31}Ti_2S_4$ at 50 °C. The achievable capacity is approximately 180 mA h g^{-1} in the first intercalation, and the Al^{3+} diffusion coefficient in cubic $Cu_{0.31}Ti_2S_4$ at 50 °C varies from ~10^{-18} to 10^{-20} cm^2 s^{-1} as Al content increases in the first Al intercalation cycle. In general, the Al^{3+} diffusion coefficient in cubic $Cu_{0.31}Ti_2S_4$ is lower than that in the layered TiS_2. The Al intercalation capacity in the second cycle is also significantly lower than that in the first cycle. However, the Al^{3+} diffusivity in the second cycle is very consistent with that in the first, which is different from what was observed in layered TiS_2. Another difference between the behaviors of layered TiS_2 and cubic $Cu_{0.31}Ti_2S_4$ is that the overpotential (difference between equilibrium potential and working potential) is greatly reduced in the second cycle for TiS_2 while the overpotential of $Cu_{0.31}Ti_2S_4$ does not change in the second Al intercalation. We hypothesize that this may also be due to the more rigid and less open crystal structure of the cubic $Cu_{0.31}Ti_2S_4$. Nevertheless, Al^{3+} ions have very low diffusivity in both titanium sulfides, which is the obstacle to facile Al intercalation−extraction. For comparison, the Li^+ diffusivities in layered TiS_2 and cubic Ti_2S_4 are approximately 10^{-9} and 10^{-10} cm^2 s^{-1} at RT[23,24] respectively, which are several orders of magnitude higher than the Al^{3+} diffusivities in those materials at 50 °C. This comparison illustrates the high-energy barrier for Al transport in these two titanium sulfide materials.

CONCLUSIONS

In summary, we examined the electrochemical Al intercalation−extraction of layered TiS_2 and cubic $Cu_{0.31}Ti_2S_4$ as potential cathode materials for rechargeable Al-ion batteries. Both titanium sulfides were evidenced to be electrochemically active toward Al intercalation−extraction, although layered TiS_2 appeared to possess better electrochemical properties than cubic $Cu_{0.31}Ti_2S_4$ as demonstrated by its higher specific capacity. Through crystallographic studies, we identified that Al^{3+} ions occupy the octahedral sites in layered TiS_2. It is also clear through GITT analysis that the main obstacle to achieving high Al intercalation capacity is the slow diffusion of Al^{3+} through the titanium sulfide crystal structures. Our future investigations will focus on shortening the Al^{3+} diffusion pathway using the nanostructure of titanium sulfides and facilitating Al^{3+} transport via ion doping at selected sites in the crystal structures.

ASSOCIATED CONTENT

Supporting Information

The Supporting Information is available free of charge on the ACS Publications website at DOI: 10.1021/acsami.7b04161.

XRD and SEM of various TiS_2 and $CuTi_2S_4$; SEM and EDS of TiS_2, $Cu_{0.31}Ti_2S_4$, and Al anode, linings, and battery case; electrochemical control experiments; cell structure schematic; SEM, EDS, and XPS spectral and electrochemical analyses of TiS_2 and $Cu_{0.31}Ti_2S_4$; CV scans; chronopotentiometry curves; and room temperature GITT data (PDF)

AUTHOR INFORMATION

Corresponding Author

*E-mail: jguo@engr.ucr.edu.

ORCID

Boniface P. T. Fokwa: 0000-0001-9802-7815

Juchen Guo: 0000-0001-9829-1202

Funding

All authors received funding from University of California, Riverside.

Notes

The authors declare no competing financial interest.

ACKNOWLEDGMENTS

This work is supported by the University of California, Riverside (startup funds allocated to B.P.T.F. and J.G.). XPS was performed at the UC Irvine Materials Research Institute (IMRI) using instrumentation funded in part by the National Science Foundation Major Research Instrumentation Program under Grant No. CHE-1338173.

REFERENCES

(1) Li, Q.; Bjerrum, N. J. Aluminum as Anode for Energy Storage and Conversion: A Review. *J. Power Sources* **2002**, *110*, 1−10.

(2) Endres, F. Ionic Liquids: Solvents for the Electrodeposition of Metals and Semiconductors. *ChemPhysChem* **2002**, *3*, 144−154.

(3) Jiang, T.; Chollier Brym, M. J.; Dube, G.; Lasia, A.; Brisard, G. M. Electrodeposition of Aluminium from Ionic Liquids: Part I - Electrodeposition and Surface Morphology of Aluminium from Aluminium Chloride ($AlCl_3$) − 1-ethyl-3-methylimidazolium Chloride ([EMIm]Cl) Ionic Liquids. *Surf. Coat. Technol.* **2006**, *201*, 1−9.

(4) Wang, H.; Gu, S.; Bai, Y.; Chen, S.; Wu, F.; Wu, C. High-Voltage and Noncorrosive Ionic Liquid Electrolyte Used in Rechargeable Aluminum Battery. *ACS Appl. Mater. Interfaces* **2016**, *8*, 27444−27448.

(5) Liu, S.; Hu, J. J.; Yan, N. F.; Pan, G. L.; Li, G. R.; Gao, X. P. Aluminum Storage Behavior of Anatase TiO_2 Nanotube Arrays in Aqueous Solution for Aluminum Ion Batteries. *Energy Environ. Sci.* **2012**, *5*, 9743−9746.

(6) He, Y. J.; Peng, J. F.; Chu, W.; Li, Y. Z.; Tong, D. G. Black Mesoporous Anatase TiO_2 Nanoleaves: A High Capacity and High Rate Anode for Aqueous Al-Ion Batteries. *J. Mater. Chem. A* **2014**, *2*, 1721−1731.

(7) Rani, J. V.; Kanakaiah, V.; Dadmal, T.; Rao, M. S.; Bhavanarushi, S. Fluorinated Natural Graphite Cathode for Rechargeable Ionic Liquid Based Aluminum-Ion Battery. *J. Electrochem. Soc.* **2013**, *160*, A1781−A1784.

(8) Gao, T.; Li, X.; Wang, X.; Hu, J.; Han, F.; Fan, X.; Suo, L.; Pearse, A. J.; Lee, S. B.; Rubloff, G. W.; Gaskell, K. J.; Noked, M.; Wang, C. A Rechargeable Al/S Battery with an Ionic-Liquid Electrolyte. *Angew. Chem., Int. Ed.* **2016**, *55*, 9898−9901.

(9) Cohn, G.; Ma, L.; Archer, L. A. A Novel Non-Aqueous Aluminum Sulfur Battery. *J. Power Sources* **2015**, *283*, 416−422.

(10) Jayaprakash, N.; Das, S. K.; Archer, L. A. The Rechargeable Aluminum-Ion Battery. *Chem. Commun.* **2011**, *47*, 12610−12612.
(11) Reed, L. D.; Menke, E. The Roles of V_2O_5 and Stainless Steel in Rechargeable Al-Ion Batteries. *J. Electrochem. Soc.* **2013**, *160*, A915−A917.
(12) Chiku, M.; Takeda, H.; Matsumura, S.; Higuchi, E.; Inoue, H. Amorphous Vanadium Oxide/Carbon Composite Positive Electrode for Rechargeable Aluminum Battery. *ACS Appl. Mater. Interfaces* **2015**, *7*, 24385−24389.
(13) Wang, H.; Bai, Y.; Chen, S.; Luo, X.; Wu, C.; Wu, F.; Lu, J.; Amine, K. Binder-Free V_2O_5 Cathode for Greener Rechargeable Aluminum Battery. *ACS Appl. Mater. Interfaces* **2015**, *7*, 80−84.
(14) Gu, S.; Wang, H.; Wu, C.; Bai, Y.; Li, H.; Wu, F. Confirming Reversible Al^{3+} Storage Mechanism Through Intercalation of Al^{3+} into V_2O_5 Nanowires in a Rechargeable Aluminum Battery. *Energy Storage Materials* **2017**, *6*, 9−17.
(15) Lin, M.; Gong, M.; Lu, B.; Wu, Y.; Wang, D.; Guan, M.; Angell, M.; Chen, C.; Yang, J.; Hwang, B.; Dai, H. An Ultrafast Rechargeable Aluminium-Ion Battery. *Nature* **2015**, *520*, 324−328.
(16) Geng, L.; Lv, G.; Xing, X.; Guo, J. Reversible Electrochemical Intercalation of Aluminum in Mo_6S_8. *Chem. Mater.* **2015**, *27*, 4926−4929.
(17) Lee, B.; Lee, H. R.; Yim, T.; Kim, J. H.; Lee, J. G.; Chung, K. Y.; Cho, B. W.; Oh, S. H. Investigation on the Structural Evolutions during the Insertion of Aluminum Ions into Mo_6S_8 Chevrel Phase. *J. Electrochem. Soc.* **2016**, *163*, A1070−A1076.
(18) Rong, Z.; Malik, R.; Canepa, P.; Sai Gautam, G.; Liu, M.; Jain, A.; Persson, K.; Ceder, G. Materials Design Rules for Multivalent Ion Mobility in Intercalation Structures. *Chem. Mater.* **2015**, *27*, 6016−6021.
(19) McKelvy, M. J.; Glaunsinger, W. S. Synthesis and Characterization of Nearly Stoichiometric Titanium Disulfide. *J. Solid State Chem.* **1987**, *66*, 181−188.
(20) Bodenez, V.; Dupont, L.; Morcrette, M.; Surcin, C.; Murphy, D. W.; Tarascon, J.-M. Copper Extrusion/Reinjection in Cu-Based Thiospinels by Electrochemical and Chemical Routes. *Chem. Mater.* **2006**, *18*, 4278−4287.
(21) Allcorn, E.; Kim, S.-O.; Manthiram, A. Lithium Diffusivity in Antimony-Based Intermetallic and FeSb−TiC Composite Anodes as Measured by GITT. *Phys. Chem. Chem. Phys.* **2015**, *17*, 28837−28843.
(22) Levi, M. D.; Lancry, E.; Gizbar, H.; Lu, Z.; Levi, E.; Gofer, Y.; Aurbach, D. Kinetic and Thermodynamic Studies of Mg^{2+} and Li^+ Ion Insertion into the Mo_6S_8 Chevrel Phase. *J. Electrochem. Soc.* **2004**, *151*, A1044−A1051.
(23) Vaccaro, A. J.; Palanisamy, T.; Kerr, R. L.; Maloy, J. T. Electrochemical Determination of the Lithium Ion Diffusion Coefficient in TiS_2. *Solid State Ionics* **1981**, *2*, 337−340.
(24) James, A. C. W. P.; Goodenough, J. B.; Clayden, N. J. Structural and NMR Study of the Lithiated Defect Thiospinels $Li_xCu_{0.07}[Ti_2]S_4$ ($0 < x < 2$). *J. Solid State Chem.* **1988**, *77*, 356−365.

DOI: 10.1021/acsami.7b04161
ACS Appl. Mater. Interfaces 2017, 9, 21251−21257